Elucidating the Mechanism of the Reverse Water–Gas Shift Reaction over Au/CeO$_2$ Catalysts Using *Operando* and Transient Spectroscopies

Marc Ziemba[†], Jakob Weyel[†], Christian Hess[*]

Eduard-Zintl-Institute of Inorganic and Physical Chemistry, Technical University of Darmstadt, Alarich-Weiss-Str. 8, 64287 Darmstadt, Germany

*email: christian.hess@tu-darmstadt.de

[†]Both authors contributed equally.

Keywords

Gold-based catalyst, CeO$_2$, Reverse water–gas shift, CO$_2$ activation, *Operando* spectroscopy

1

Abstract

The reaction mechanism of the reverse water–gas shift reaction (rWGSR) over Au/ceria catalysts was investigated by monitoring the catalyst dynamics and reaction intermediates using *operando* and transient spectroscopies, as well as by DFT calculations. Combined *operando* Raman and UV-Vis spectroscopic analysis allows establishing a correlation between subsurface oxygen vacancies and catalytic activity. Comparison of different ceria support materials, i.e., polyhedra and polycrystalline sheets, reveals that the defect concentration is not rate-determinant. Using transient DRIFTS, we are able to identify individual steps of hydrogen dissociation on supported gold and to gain detailed insight into the reduction of CO_2 via formate and carbonate formation. It is demonstrated that CO_2 reduction is influenced by the surface pretreatment. Considering all spectroscopic findings, we propose an associative mechanism via carbonate and formate intermediates as the main route for the rWGSR over Au/ceria(111) catalysts, while a redox mechanism plays only a minor role.

Graphical Abstract
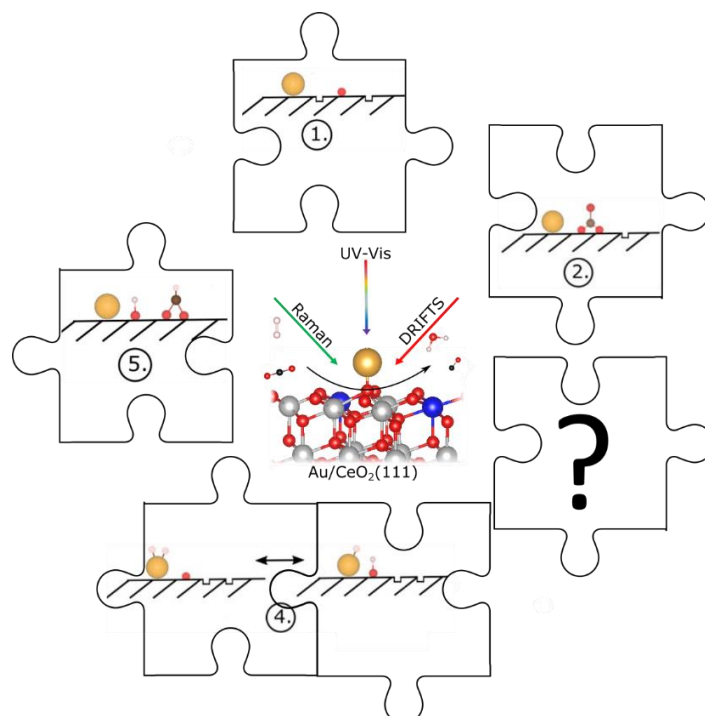
1. Introduction

The ever-increasing levels of CO_2 emissions[1] and the resulting impact of the greenhouse effect are the main reasons for the importance of dealing with CO_2, while solutions to stop its further release into the atmosphere continue to be sought after. In an increasing number of CO_2 capture technologies, its activation and use as a C1 source is an attractive strategy.[2] It is of particular interest to use CO_2 as a non-fossil source for the production of syngas, owing to its versatility and relevance for a multitude of applications. In this context the reverse water–gas shift reaction (rWGSR) plays an important role in the energy sector, allowing CO_2 to be converted first to CO and then to liquid fuels via CO hydrogenation (Fischer–Tropsch process).

While noble metal–loaded CeO_2 catalysts have been shown to be active for the rWGSR,[3,4] their mode of operation (redox vs associative mechanism) is still a matter of debate. For example, previous studies on Pt/CeO_2 catalysts have shown that intermediates such as carbonates or formates play an important role in the reaction, pointing to an associative mechanism.[5,6] In contrast, the water-gas shift reaction at 300 °C proceeds largely via a redox mechanism.[7] Considerable catalytic activity as well as the appearance of intermediates such as formates or bidentate carbonates was also reported for Cu/CeO_2 catalysts.[8] In this context, a facet dependence of the ceria support was reported, with the $CeO_2(110)$ surface showing a much higher activity than the $CeO_2(111)$ surface.[8] In contrast, experiments on the bare supports, which become active at temperatures >550 °C,[9] have shown that the effect of the surface termination is much smaller,[9] highlighting the importance of the metal–support interaction.

Regarding other supports, recent *operando* studies of the rWGSR over gold-loaded catalysts, comparing a redox active (Au/TiO_2) with an inactive (Au/Al_2O_3) support, are of interest in the context of the present study.[10] In particular, the reaction over Au/Al_2O_3 is shown to occur via intermediates such as formates, while for the Au/TiO_2 catalyst a redox mechanism involving the formation of hydroxycarbonyls has been postulated, following earlier studies on copper- and gold-loaded $TiO_2(110)$ catalysts during the water–gas shift reaction.[11] With increasing temperature, the associative mechanism is found to contribute more strongly, due to more facile decomposition of adsorbates such as carbonates and formates, thereby releasing CO.[10]

This study will focus on Au/CeO_2 catalysts that are known to be active for the rWGSR[12,13] and water–gas shift reaction (WGSR).[14–17] While previous studies have demonstrated that Au/CeO_2 catalysts[12] as well as bare ceria[18,19] can be re-oxidized by CO_2, indicating a redox mechanism, the role of adsorbates/reaction intermediates has not been

clarified yet. In this context, it is of particular interest to explore the role of gold during the re-oxidation process and its contribution during rWGSR. For LT-WGSR and CO oxidation it has previously been shown that the gold/ceria interface and size distribution have an influence on the catalytic activity.[20,21] Using XAS and DRIFTS during LT-WGSR gold was found to be metallic,[22] but under reductive conditions or in long-term studies agglomeration of surface gold atoms to small gold particles can occur.[23] Applying *operando* SSITKA-mass spectrometry-DRIFTS to the LT-WGSR over a 0.5 wt% $Pt/Ce_{1-x}La_xO_{2-\delta}$ catalyst has revealed that the active species is not only formed on the Pt particle but also in its environment,[24] which again underlines the importance of the metal-support interaction. In addition, previous studies have shown that hydrogen dissociation on stoichiometric ceria, which leads to the formation of two surface hydroxides, requires temperatures >400 °C.[25] However, surface oxygen defects significantly affect the H_2 adsorption, giving rise to increased heterolytic dissociation (Ce-H and OH).[25,26] On Au/CeO_2 catalysts, heterolytic dissociation is feasible at 150 °C, leading to a hydroxide and a gold hydride species.[27] Furthermore, studies on different gold supported materials have shown that an increase in the gold loading results in a higher surface hydroxide concentration, thus providing direct evidence for a gold-catalyzed H_2 dissociation.[28]

To elucidate the rWGS reaction mechanism in detail, we employed combined *operando* Raman and UV-Vis as well as transient DRIFTS measurements, supplemented by quasi *in situ* XPS, enabling us to address the support and (transient) adsorbate dynamics, as well as the surface state of Au/CeO_2 catalysts, in an integrated manner. We obtain insight into the role of the support by using ceria with two different particle shapes, i.e., polycrystalline ceria and ceria polyhedra. While polyhedra terminate exclusively with the $CeO_2(111)$ surface, the polycrystalline ceria, which resembles sheets, also contains stepped sites. Previous studies have shown a positive effect of stepped sites on the activity during CO oxidation over Au/CeO_2 catalysts.[29]

2. Experimental Section

2.1 Catalyst Preparation

Polycrystalline ceria sheets were prepared by decomposition of cerium nitrate as described in previous studies.[15,30] Briefly, $Ce(NO_3)_3 \cdot 6H_2O$ (Alfa Aesar, 99.5 %) was calcined at 600 °C (6 °C/min) for 12 h. After cooling to room temperature, the powder was sieved (200 μm) and calcined again using the same protocol. Ceria polyhedra were obtained commercially (Sigma

Aldrich, <25 nm (BET)). Gold was loaded onto ceria by electrolyte deposition using a 10^{-3} M HAuCl$_4$ ·3H$_2$O solution (Carl Roth, 99.9 %), as described in detail elsewhere.[15,30]

2.2 Catalyst Characterization

2.2.1 *Operando* Spectroscopy

Combined *operando* Raman and UV-Vis spectra as well as the catalytic activity were measured with a previously described experimental setup.[14,15,31,32] Briefly, for the *operando* measurements, about 20–25 mg of the sample was placed in a stainless steel sample holder (8 mm diameter, 0.5 mm depth). Due to the cell geometry and as the catalyst sample is overflowed by the gases, the amount of catalyst has hardly any influence on the activity. The sample temperature was determined by means of a Ni/Cr-Ni thermocouple (type K), which was located at the sample holder close to the catalyst. Measured temperatures deviated by a maximum of 3 °C from the set temperatures in a constant gas stream. The catalyst temperature was set to 250 °C in all measurements. Raman spectra were recorded with an HL5R transmission spectrometer (Kaiser Optical), using a frequency-doubled Nd:YAG laser (Cobolt) for excitation at 532 nm. The laser power at the position of the sample was 1 mW, as measured with a power meter (Ophir). The spectral resolution was specified as 5 cm^{-1} and the band position stability was better than 0.3 cm^{-1}. Spectra of the gold-loaded catalysts were recorded with an exposure time of 225 s and 2 accumulations and those of the bare samples with an exposure time of 150 s and 3 accumulations. For all measurements a cosmic ray filter and an auto new dark correction were applied, resulting in a total measuring time of about 1800 s for the bare and gold-loaded samples. All Raman spectra reported in this work were normalized to the band with the highest intensity, i.e., the F$_{2g}$ band. The given F$_{2g}$ positions were determined by curve fitting using Lorentzian functions.

UV-Vis spectra were recorded in diffuse reflection using an AvaSpec ULS2048 spectrometer (Avantes) equipped with a deuterium lamp and a halogen discharge lamp. Spectra were taken before and after a Raman spectrum. The total measuring time was 60 s, resulting from 200 runs with an exposure time of 300 ms each. As white standard, magnesium oxide powder (Sigma Aldrich) was employed, which shows no absorption within 170–1100 nm.

The gases CO$_2$ (99.999 %, Westfalen), H$_2$ (99.999 %, Westfalen), and argon (99.996 %, Westfalen) were dosed by digital mass flow controllers (MFCs, Bronkhorst). Gas atmospheres of 10 vol% H$_2$/Ar, 2 vol% CO$_2$/Ar, and 4 vol% H$_2$/2 vol% CO$_2$/Ar for reactive conditions were

applied at a total flow rate of 100 mL/min. All gas compositions are balanced in argon to keep the turnover low and to eliminate the influence of possible transport effects thus allowing to focus on the reaction mechanism. To analyze the gas phase and its composition, a Fourier transform infrared (FTIR) spectrometer (Tensor 20, Bruker) was installed at the outlet of the reaction cell. The resolution was 4 cm^{-1}, and the measurement time was 1 minute, in which 125 spectra were accumulated. Using calibration curves, the concentration of CO was calculated, allowing the conversion of CO_2 to CO to be determined. The catalytic activity is the ratio of the amount of CO, as measured by FTIR at the outlet of the cell, to the amount of dosed CO_2. The activity of the empty cell, which showed a CO_2 conversion of 4.2 %, was taken into account when calculating the catalyst activities given in the following. Please note that this background activity is a result of the cell specifications and has been shown to be reproducible.

2.2.2 Transient DRIFTS

Diffuse reflectance IR Fourier transform spectroscopy (DRIFTS) was performed on a Vertex 70 (Bruker) FTIR spectrometer equipped with a liquid nitrogen cooled mercury cadmium telluride (MCT) detector and a commercial reaction cell (Praying Mantis™ High Temperature Reaction Chamber, Harrick Scientific Products) with infrared transparent KBr windows, as described previously.[30,33]

As background, the catalyst itself was employed after a 15-minute exposure at 250 °C to H_2 (4 mol%) or CO_2 (2 mol %) or the reaction mixture (4 mol% H_2 and 2 mol% CO_2, balanced with argon; total gas flow: 100 mL/min). For transient measurements we employed the rapid scan mode extension of Bruker's spectrometer software OPUS 7.2. Spectra were acquired within 850–3800 cm^{-1}, utilizing a resolution of 0.5 cm^{-1} and an aperture of 8 mm. The mirror speed was set to 40 kHz. A Valco Instruments 4/2 valve (Model E2CA, version ED), communicating with the Vertex 70, was employed to rapidly switch between gas flows.

In transient DRIFTS experiments, the gas phase was switched immediately after the background spectrum had been recorded, commencing the measurements. A spectrum was obtained every 5 s and consisted of an average of six individual spectra, each based on five interferograms. One measurement series took 6 minutes.

3. Results and Discussion

3.1 Catalyst characterization and performance

The ceria nanoparticles were first characterized using BET and TEM (for details see Figure 1 and SI, Figures S1, and S2). The commercial sample contains particles in the form of polyhedra with a specific surface area of 36 m^2/g and a pore volume of 0.08 cm^{3}g^{-1}, whereas the sample prepared by decomposition of cerium nitrate, as described previously,[14] contains particles with a sheet shape with a surface area of 57 m^2/g and a pore volume of 0.17 cm^{3}g^{-1}. Both samples exhibit a CeO$_2$(111)-terminated surface, but the sheets show additional stepped CeO$_2$(111) sites (see Figure 1).[14] Using ICP-OES, the gold loading was determined as 0.31 wt% for the sheets and 0.27 wt% for the polyhedra. In our previous study on Au/CeO$_2$(111) sheets, the CO-Au vibrations measured by DRIFTS showed a large dispersion of gold due to presence of single atoms and/or smaller clusters, which we assume to be the prepared state also in this study.[33] Contaminations caused by the synthesis, e.g. nitrogen or chlorine, can be excluded within the sensitivity of the XPS measurements.
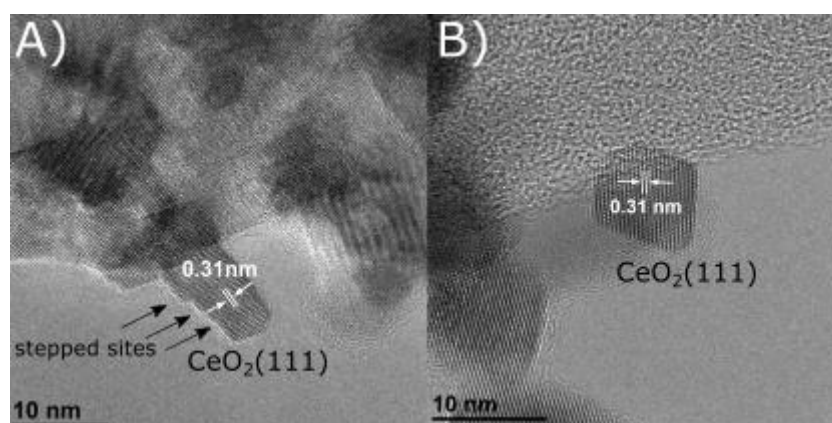

Figure 1: Detailed TEM images of **A)** ceria sheets and **B)** ceria polyhedra. The white arrows indicate the separation of the lattice planes in the direction of the particle surface. Figure 1A was modified from Ref. [14].

As summarized in Table 1, both the bare and gold-loaded ceria samples show conversion of CO$_2$ upon exposure to reaction conditions (4 % H$_2$, 2 % CO$_2$, Ar; 100 mL/min) at 250 °C. For the unloaded polyhedra and sheets, activities of 2.2 % and 1.6 % were determined, respectively, while the gold-loaded samples showed significantly higher activities of 5.3 % (Au/polyhedra) and 5.4 % (Au/sheets). It is noteworthy that the polyhedra yield a higher CO$_2$ conversion despite their lower surface area. The activity of the gold-loaded samples, on the other hand, does not

show a significant difference within the experimental error. In comparison to a previous study on 2.4 wt% Au/CeO_2 the activity is in the same range (4.8×10^{-8} mol_{CO}/s, 240 °C) as reported here,[12] while compared to other ceria-based materials,[4] our Au/CeO_2 catalysts show rather high activity considering the low temperature and higher CO_2 concentration. A 2% Pt/CeO_2 catalyst (Johnson Matthey) has previously been reported to show a conversion of 13.7 % at 225 °C, but it should be noted that a lower flow rate of 40 mL/min and a CO_2:H_2 ratio of 1:4 was used, thus preventing a direct comparison of the activity data.[34]

Table 1: Catalytic activity during rWGSR over bare ceria and gold-loaded ceria samples using a feed of $H_2/CO_2/Ar$ (4 % H_2, 2 % CO_2, Ar; 100 mL/min) at 250 °C. The catalytic activity was measured after at least 1 hour time-on-stream.

Sample	CO_2 conversion	
	%	mol_{CO}/s
CeO_2 sheets	1.6	2.2×10^{-8}
CeO_2 polyhedra	2.2	3.0×10^{-8}
0.31 wt% Au/CeO_2 sheets	5.4	7.3×10^{-8}
0.27 wt% Au/CeO_2 polyhedra	5.3	7.2×10^{-8}

3.2 Role of Au and CeO_2

Figure 2 depicts combined Raman and UV-Vis data of bare and gold-loaded sheets and polyhedra, recorded at 250 °C for different gas atmospheres. As discussed below, the Raman F_{2g} positions and the change in UV-Vis absorption at 550 nm both reflect the reduction of the ceria support. In the following, we will first focus on the F_{2g} position, which has previously been shown to be a good indicator for subsurface oxygen defects.[14,15,32] Compared to the starting F_{2g} positions in argon, it is noticeable that the gold-loaded samples are red-shifted with respect to the unloaded samples, evidencing that the gold-loaded samples possess a larger number of oxygen defects. Based on this observation, one may expect the gold-loaded samples to be more reducible, which is confirmed by changing the gas phase to H_2. In fact, for the gold-loaded samples a significantly larger redshift than for the unloaded samples is detected, whereby the shift is greatest for the sheets. This behavior demonstrates that polyhedra and sheets are characterized by a different defect formation energy, which is smaller for the sheets. When switching to reaction conditions, all samples show only slight changes, which are within

8

the experimental error, which is why no conclusions should be drawn at this point. However, upon switching to argon, a blueshift is observed, which is indicative of an oxidation of the subsurface and can be explained by a diffusion of oxygen from the bulk to the surface. Such an oxygen diffusion was confirmed by $H_2^{18}O$ experiments in our previous studies on the WGSR over Au/ceria catalysts.[14,15] Our results show that reaction intermediates formed during reaction conditions can decompose or desorb in argon, leaving a surface oxygen vacancy and thus promoting an oxygen diffusion from the bulk to the (sub)surface, which results in a F_{2g} blueshift.
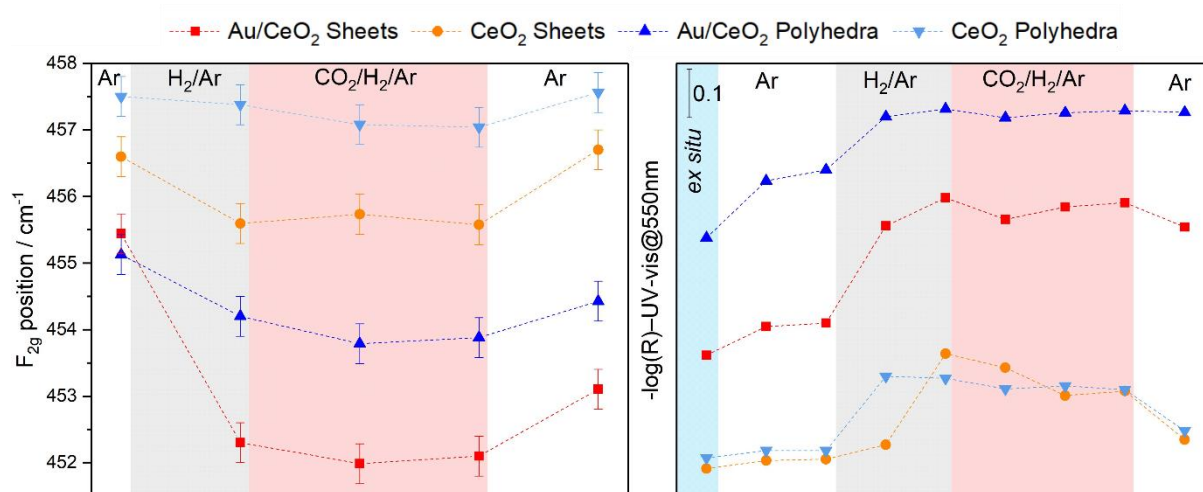

Figure 2: *In situ* and *operando* Raman (left) and UV-Vis (right) results for Au/CeO$_2$ sheets and Au/CeO$_2$ polyhedra together with the corresponding bare support materials recorded during the indicated gas exposures at 250 °C and at a total flow rate of 100 mL/min, except for the *ex situ* spectra, which were taken at 25 °C. The measurement error for the F_{2g} position is indicated. The sample was exposed to each gas phase for about 30 min except for the reaction phase, which was present for 1 hour. For details see text.

The absorption increase at 550 nm, which can be attributed to a charge transfer from Ce^{3+} to Ce^{4+},[35] allows the change in the oxidation state of the support to be monitored, i.e., the extent of ceria reduction. Comparison of the unloaded and the gold-loaded samples reveals that gold-containing ceria shows a higher absorption at 550 nm already under *ex situ* conditions (see Figure 2), which can be explained by the presence of metallic gold giving rise to surface plasmons absorbing in this range.[36] Accordingly, the higher absorption of the gold-loaded polyhedra can be explained by their higher fraction of metallic gold, which is confirmed by the

9

Au 4f photoemissions (see below) and the *ex situ* UV-Vis spectra (see Figure S3). Upon heating to 250 °C under argon, the gold-loaded samples show an increase in absorption, indicating that the presence of gold can reduce the defect formation energy. When the feed is switched to hydrogen, all samples show an increase, consistent with the Raman results. Interestingly, this reduction-induced increase is also detected for the unloaded polyhedra, but was hardly detected in the Raman F_{2g} shift, which can be explained by the different information depths of the two methods. Upon exposure to reaction conditions, a slight decrease in absorption can be seen in all samples, resulting from ceria oxidation, whereas switching to argon leads to a more pronounced re-oxidation of the support, in agreement with the Raman results, except for the gold-loaded polyhedra. The UV-Vis behavior of the gold-loaded polyhedra may be explained by the higher fraction of metallic gold and its partial agglomeration during exposure to reducing conditions. Briefly summarizing, all unloaded and gold-loaded samples are subject to gas-phase-dependent oxygen dynamics. A comparison of the extent of ceria reduction, as observed by *operando* Raman and UV-Vis spectroscopy, with the rWGSR activity data shows that the role of the support reducibility for the reaction mechanism needs to be further explored.

To gain more detailed insight into the catalysts' vibrational and electronic structure under reductive, reactive, and oxidative conditions, Figure 3 depicts Raman spectra (left panel) and UV-Vis specra (right panel) of the gold-loaded samples during exposure to H_2/Ar, reaction conditions, and CO_2/Ar. In the Raman spectra, the band at 243 cm^{-1}, originating from the longitudinal mode of surface oxygen, and the oxygen defect-related band at 550 cm^{-1} are of particular interest.[37] The surface mode shows an increase in intensity during CO_2 exposure, which is more pronounced for the sheets, demonstrating that the surface of the sheets can be re-oxidized more efficiently under CO_2 atmosphere than that of the polyhedra. It is difficult to make statements about the intensity of the defect band as the background changes with the gas atmosphere and thus both re-oxidation and background changes are likely to have an effect on the intensity of the defect band. However, as can be seen from Figure 3A, the 550 cm^{-1} band is more pronounced for the polyhedra and its shape changes upon exposure to CO_2. The broad band at 1170 cm^{-1} is caused by the 2LO overtone,[37] whereas additional features above 1250 cm^{-1} may originate from carbonaceous adsorbates. This aspect will be investigated in more detail using DRIFTS (see below).

The UV-Vis spectra in Figure 3B show that under CO_2 atmosphere the absorption decreases from about 450 nm on. This effect is more pronounced for the sheets, which can be explained by more facile surface oxidation of the sheets, fully consistent with the intensity increase of the Raman longitudinal surface oxygen mode at 243 cm^{-1} (see above). The increase

in oxidation during exposure to CO_2 also influences the band edge. In fact, as shown in the inset of Figure 3B, the absorption becomes wider due to the larger band gap, originating from the decrease in Ce^{3+}.[35] Upon switching from H_2 to reaction conditions no significant change in the gold surface plasmon region (~550 nm) was observed, indicating that about the same degree of gold agglomeration is present under both conditions. In this context, it should also be mentioned that previous studies on Au/CeO_2 have shown that H_2 treatment at 200 °C already reduces all cationic gold to metallic gold.[38]
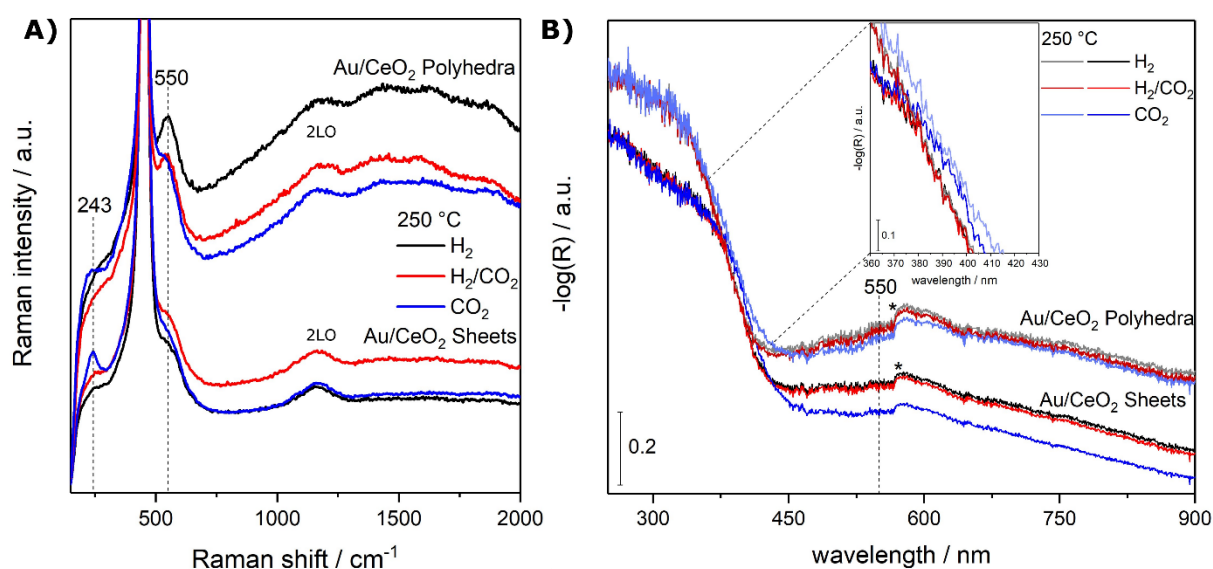

Figure 3: *Operando* **A)** Raman and **B)** UV-Vis spectra of Au/CeO_2 sheets (bottom) and Au/CeO_2 polyhedra (top). The spectra were recorded at 250 °C, at a total flow rate of 100 mL/min, and during gas exposures to H_2 (10 %), H_2/CO_2 (4 %/2 %) and CO_2 (2 %). In the Raman spectra the high-intensity F_{2g} peak was cut off to allow an enlarged view of the other features. The inset in the right panel provides an enlarged view of the absorption within 360-430 nm.

Next, the gold-loaded samples were alternately exposed to H_2, CO_2, and reaction conditions, and monitored by combined *operando* Raman and UV-Vis spectroscopy. The results for the F_{2g} position, the absorption at 550 nm, and the gas-phase IR signal are summarized in Figure 4. The spectroscopic data clearly shows that CO_2 is able to re-oxidize pre-reduced gold-loaded ceria, which can then be reduced again by H_2. The simultaneous gas-phase analysis reveals the formation of H_2O during H_2 treatment, while subsequent treatment

with CO_2 leads to CO and H_2O formation (see Figure 4), demonstrating that hydrogen must still be present on the surface, e.g. as adsorbed water or hydroxide. This observation will be confirmed by the DRIFTS data (see below). Likewise, after CO_2 treatment followed by exposure to H_2, CO and H_2O are formed (see Figure 4), which shows the presence of surface carbon species, which only desorb when hydrogen is available. We can rule out residual H_2 or CO_2 as a potential source for the gas-phase signals, as the residence time is about 1 minute but the effects continue for more than 10 minutes. Thus, the results so far would be consistent with a (combined) redox and associative mechanism.

In Figure 4 it is noticeable that the changes in F_{2g} position and 550 nm absorption are larger for the sheets, underlining their higher redox activity. Interestingly, polyhedra and sheets are characterized by different reduction levels after H_2 treatment (see F_{2g} positions), but show the same F_{2g} position upon exposure to CO_2. This behavior may be an indication that reduced ceria can only be oxidized to a limited extent by using CO_2. Despite equal F_{2g} positions, different absorptions at 550 nm are observed, which can be explained by different fractions of metallic gold clusters.

In the following, we will examine more closely the effect of the pretreatment (H_2 or CO_2) on the reaction process. When the atmosphere is switched from H_2 to reaction conditions, the UV-Vis spectra show a slight decrease in 550 nm absorption and the Raman spectra a small F_{2g} redshift (see Figures 4 and S4). However, these changes are too small to make a definitive statement. Nevertheless, the situation is different in the case of the CO_2 pretreatment, where the two samples show a pronounced reduction when the reaction conditions are switched on, as indicated by the F_{2g} redshift and the increase in 550 nm absorption, both of which are significantly higher for the sheets. Comparison of the activity data in Figures 4 and S4 reveals that after pretreatment with CO_2 both samples yield a 0.5 % smaller conversion. This behavior suggests that the reaction occurs preferentially over a reduced surface and, as indicated by the F_{2g} shift, lattice oxygen is involved in the reaction mechanism. Another aspect that may affect the activity could be the formation of stable adsorbates during CO_2 treatment, thus blocking active sites. This aspect of the influence of pretreatment will be addressed later in the context of our transient measurements. After reaction conditions, the feed was switched to argon as in the previous measurements (see Figure 2), which leads to a re-oxidation, whereby the observed changes are significantly larger for the sheets, again showing their increased oxygen mobility.
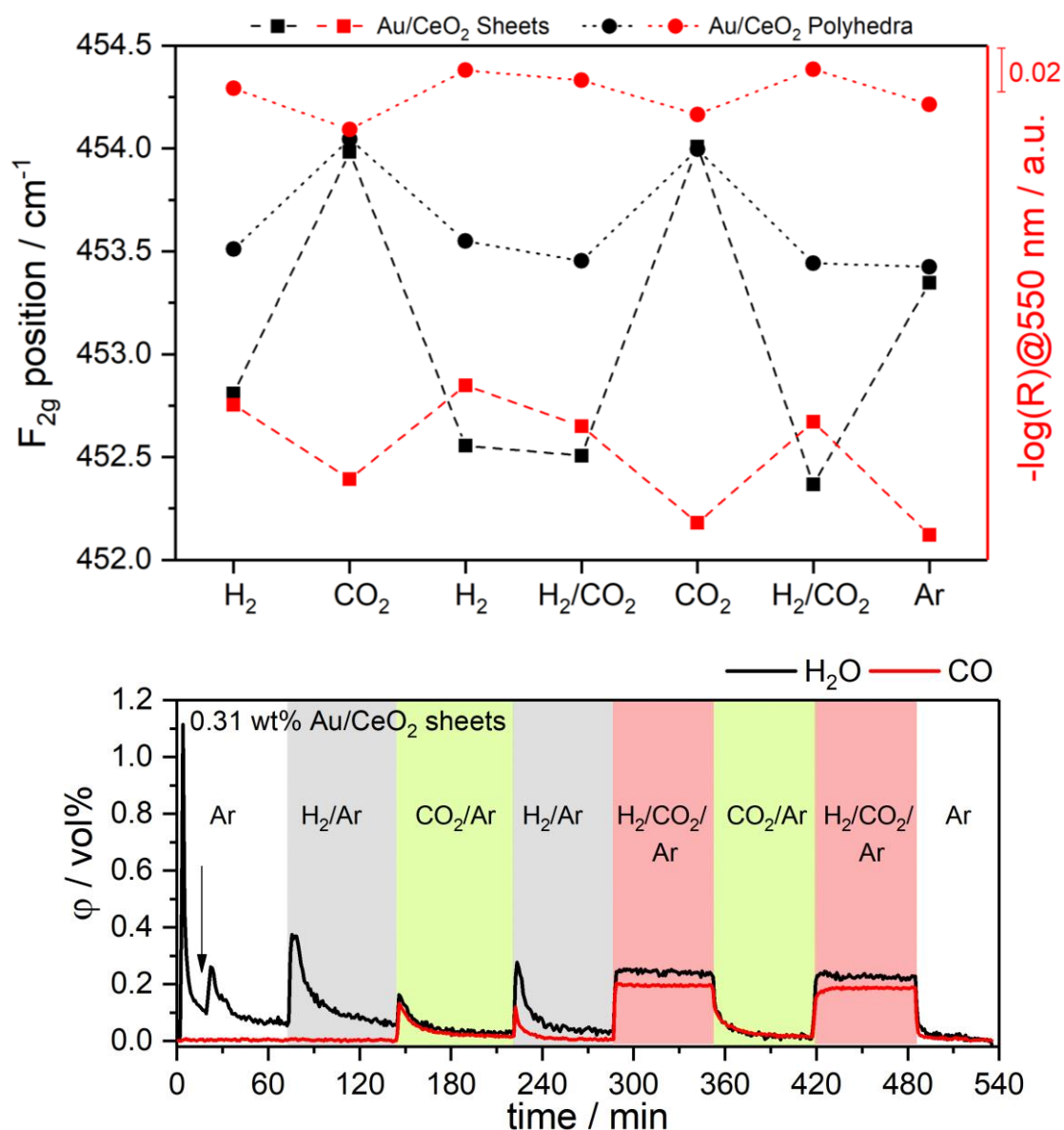
Figure 4: Top: *Operando* Raman and UV-Vis results of Au/CeO₂ sheets and Au/CeO₂ polyhedra during exposure to H_2 (10 %), CO_2 (2 %), H_2/CO_2 (4 %/2 %), and argon at 250 °C and a total flow rate of 100 mL/min. The data were obtained by averaging two Raman spectra and three UV-Vis spectra per gas phase, except for argon, where the results from only one Raman spectrum and two UV-Vis spectra were used. **Bottom**: Gas-phase IR analysis of Au/sheets. The corresponding data for Au/polyhedra are shown in Figure S4. The increased water concentration in the first few minutes is due to the purging of the cell. The cell was heated to 250 °C, starting after 19 minutes (see black arrow), leading to water desorption and thus an increase in the H_2O concentration.

To investigate the changes in oxidation state of the surface after exposure to different gas atmospheres, quasi *in situ* XPS was applied. In these measurements, XPS spectra were recorded after synthesis, H_2 pre-treatment, and reaction conditions without exposure to air when transferring the samples from the pre-treatment/reaction cell to the analysis chamber. It should be mentioned that XPS probes exclusively surface properties, in contrast to Raman and UV-Vis spectroscopy. First of all, XPS analysis did not reveal a significant increase in the surface carbon concentration after reaction conditions (not shown). Hence there is no indication for coking during reaction. As a measure of the surface oxidation state, Table 2 and Figure S8 depict the O:Ce ratios of the gold-loaded samples, while the corresponding Au 4f photoemissions are shown in Figure S9. Starting with the O:Ce ratios of the as-prepared samples, both Au/sheets and Au/polyhedra are characterized by approximately the same O:Ce ratio of 1.97. This is indicative of the presence of surface oxygen defects, and considering that adsorbates such as carbonates or water are still present after synthesis (see outgassing process in Figure 4), the actual defect content after synthesis will be higher than this value suggests.

Upon treatment with 10 % H_2 at 250 °C, a decrease in the O:Ce ratio is observed for both samples, which can readily be explained by a surface reduction due to water formation, as evident from the gas-phase IR measurements (see Figures 4 and S4). This behavior is also consistent with the F_{2g} redshift and the 550 nm absorption increase discussed above (see Figure 2). However, upon closer inspection, it can be seen that the stoichiometry change is smaller for the sheets than for the polyhedra, suggesting a lower defect concentration at the surface of the sheets.

At first glance, this observation seems to be in conflict with the Raman and UV-Vis measurements that probe the subsurface. However, the apparent contradiction can be resolved when taking into account the oxygen mobility between surface and subsurface and the fact that oxygen defects are first formed at the surface. In fact, according to the Raman and UV-Vis results, an exchange between surface and subsurface/bulk must have taken place upon switching from reactive to argon atmosphere, because all samples are subject to an F_{2g} blueshift and absorption decrease, despite the inert conditions (see Figure 4). As these changes are always larger for the sheets, a larger mobility of lattice oxygen in sheets is expected than for the polyhedra. As a consequence of the more facile transfer of oxygen from the subsurface/bulk to the surface, the overall change in the O:Ce surface ratio is smaller for the sheets.

After analysis of the reduction treatment, the sample was transferred to the reaction chamber under absence of air and exposed to reaction conditions, followed by another XPS measurement. As shown in Table 2 and Figure S8, a further decrease of the O:Ce ratio is

detected, but these changes are within the error of the experiment. To this end, we cannot exclude the loss of adsorbates formed under reaction conditions when transferring the sample to the XPS analysis chamber under vacuum conditions. In fact, transient DRIFT spectra clearly show that reaction intermediates desorb immediately after the reaction conditions are stopped by switching off one reactant (see Figure S6). For these reasons, the quasi *in situ* analysis after reaction conditions needs to be treated with caution.

Table 2: Surface O:Ce ratios as obtained from the XPS analysis of gold-loaded ceria sheets and polyhedra.

Pretreatment	O:Ce ratio
0.31 wt% Au/CeO_2 sheets	
None (as prepared)	1.97 ± 0.07
30 min H_2 (10 %), 250 °C	1.83 ± 0.08
1 h H_2/CO_2 (4 %/2 %), 250 °C	1.75 ± 0.09
0.27 wt% Au/CeO_2 polyhedra	
None (as prepared)	1.97 ± 0.08
30 min H_2 (10 %), 250 °C	1.50 ± 0.08
1 h H_2/CO_2 (4 %/2 %), 250 °C	1.39 ± 0.06

Next, the state of gold will be addressed based on the Au 4f photoemissions. Due to the low gold loading, a quantitative analysis is challenging (see Figure S9), but qualitative statements can still be made. Independent of the pretreatment and sample, the state of the gold does not change significantly and metallic or negatively charged gold is present independent of the pretreatment, since the central Au $4f_{7/2}$ binding energy never exceeds values of 84.5 eV. However, a comparison between polyhedra and sheets shows that the signals of polyhedra are at slightly lower binding energies (~0.4 eV), which could indicate more metallic gold, in agreement with the UV-Vis results. In this context, besides the state of gold the presence of potential gold adsorbates should be taken into account. The latter will be addressed by transient DRIFT spectra, as described in the following.

3.3 Transient surface analysis

To gain insight into possible adsorbates during the reaction, transient DRIFT spectra of unloaded and gold-loaded ceria catalysts were recorded, by using spectra of the catalysts under H_2 or CO_2 as background. As the background is measured either in H_2, CO_2 or H_2/CO_2, negative signals can occur due to non-stable intermediates. These negative signals are important indicators providing information about the reversibility as well as possible intermediates, which are only formed under reaction conditions. After the background had been recorded, CO_2 or H_2 was added to the constant feed of H_2 or CO_2, thus switching to reaction conditions, and transient DRIFT spectra were taken every 5 s to monitor the temporal evolution of the adsorbates. By recording the gas-phase composition together with transient DRIFT spectra we confirmed the formation of CO and H_2O under reaction conditions. Figure 5 depicts transient DRIFT spectra recorded 6 minutes after switching on the H_2 (A) and CO_2 (B) flow. The same experiments were also performed in reverse, i.e., the catalysts were exposed to reaction conditions and then one reactant was removed (see Figure S6). Both experiments give comparable results, with the difference that the latter measurements show an inverse trend for the same signals. This reversibility underlines that the corresponding adsorbate bands must be related to reaction intermediates. We also recorded transient DRIFTS after 2h, largely resembling the behavior after 6 min, and performed modulation excitation (ME) DRIFTS (for details see SI), which show the same bands as our transient DRIFTS experiments, further supporting our claim that the observed bands are associated with reaction intermediates.[39]

When comparing the sheets and polyhedra in both experiments with and without gold loading, the same overall trends are observed. However, it is noticeable that the signals are sharper for the polyhedra, which contain only one clearly defined surface termination, i.e., $CeO_2(111)$, thus limiting the number of possible adsorbates compared to the sheets which terminate mainly with the $CeO_2(111)$ facet, but exhibit additional steps. Despite the latter differences, the similarities of the adsorbate bands detected for polyhedra and sheet samples point to a dominance of $CeO_2(111)$-related vibrational features. Therefore, the signals of ceria sheets and polyhedra that can be seen in Figure 5 will be discussed together in the following.

To trace species related to the reaction, one needs to identify IR bands, which exhibit comparable intensity changes in both experiments, i.e., when either H_2 or CO_2 is switched on. Comparison of the spectra of the gold-loaded sheets and polyhedra in Figure 5 reveals that this is obviously the case for the C-H stretching signal at 2838 cm^{-1} as well as its minor neighboring peaks at 2712 cm^{-1} and 2945 cm^{-1}, which are all assigned to bridged/bidentate formate species in agreement with the literature.[40–43]
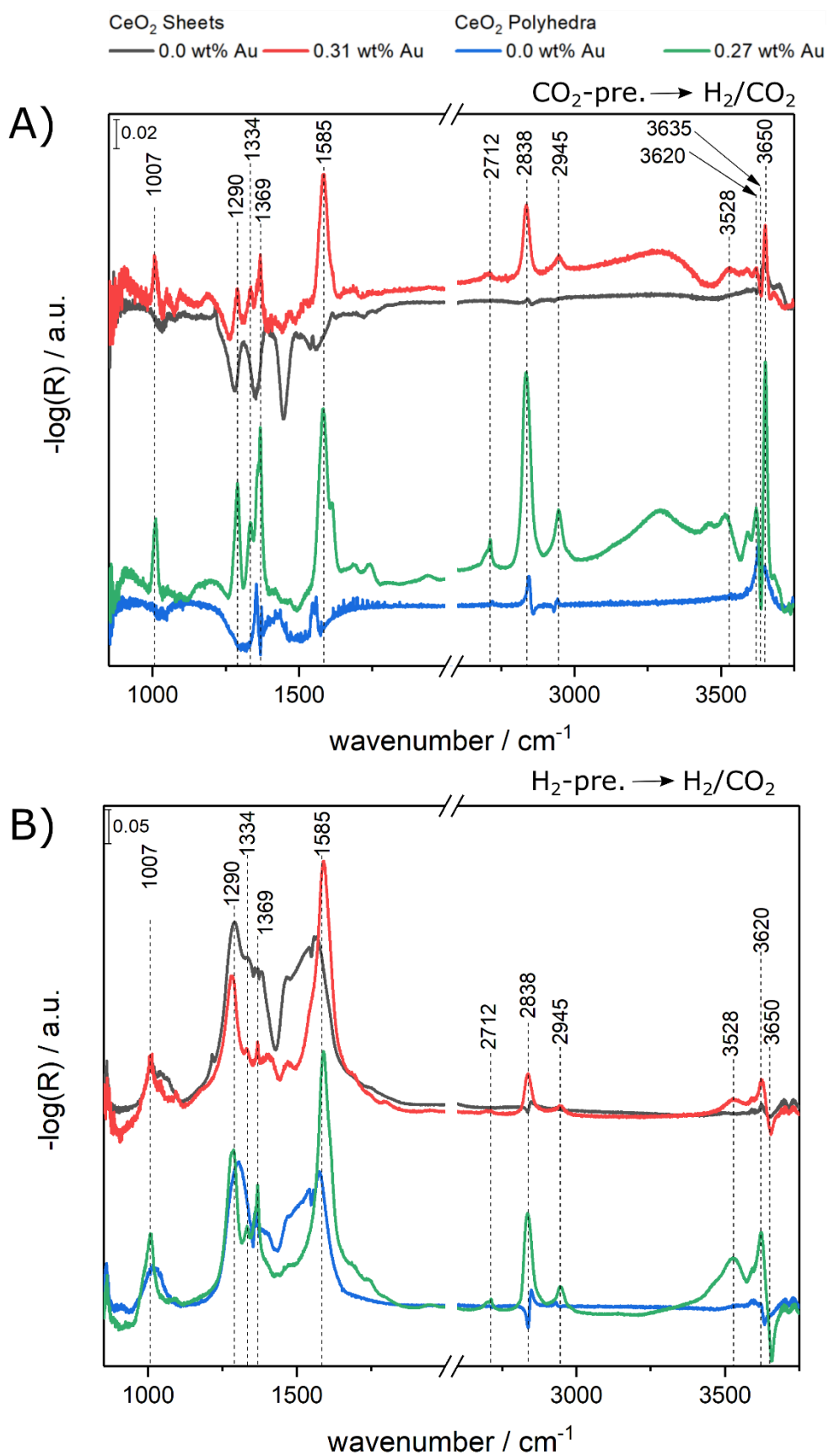
16

Figure 5: Transient DRIFT spectra of bare and gold-loaded polyhedra and sheets. The spectra were recorded after pretreatment in H_2 (4 mol%) or CO_2 (2 mol%) balanced in argon at 250 °C at a total gas flow of 100 mL/min. Prior to the measurements **A)** the H_2 supply was switched on while CO_2 remained constant or **B)** the CO_2 supply was switched on while H_2 remained constant. Shown are only the last spectra of a measurement series with a duration of 6 min. As background, spectra of the catalyst after 15-minute exposure to either H_2 (4 mol%) or CO_2 (2 mol %) at 250 °C were employed.

Further confirmation of the presence of formate species may arise from the identification of their complete vibrational pattern, including the region below 2000 cm^{-1}. In this region, signals appear at about 1007 cm^{-1}, 1290 cm^{-1}, 1334 cm^{-1}, 1369 cm^{-1}, and 1585 cm^{-1} in both experiments, which, except for the 1290 cm^{-1} feature, all coincide with the expectations for bridged formate species.[40,41] Regarding bare ceria, formate-related C-H signals can be detected unambiguously for polyhedra only. The identification of other formate bands, identified previously for gold-loaded samples, is hampered by the appearance of negative signals in the carbonate region for the bare samples when switching on H_2 (see Figure 5A), as will be discussed below. When switching on CO_2, besides the increasing C-H signal at 2848 cm^{-1}, a nearby negative signal at 2838 cm^{-1} is observed (see Figure 5B). This indicates that a small part of the formate species may either undergo structural changes or may be subject to changing surroundings, possibly induced by the different redox properties of the reductive gas environment. Therefore, an additional experiment was performed, in which the gas phase was switched between reactive and reducing conditions (see Figure S5). The observed 10 cm^{-1} redshift of the C-H signal at 2848 cm^{-1} upon reduction is fully consistent with the results in Figure 5, thus confirming the above hypothesis, while the continuous shift behavior evidences the reversibility of the gas phase-induced changes.

Concerning gold-loaded ceria, the two signals at about 1007 cm^{-1} and 1585 cm^{-1}, together with the intense and characteristic band at 1290 cm^{-1}, suggest the presence of a carbonate species. However, the features at around 1007 cm^{-1} and 1585 cm^{-1} coincide with those of formate (see above). The latter feature furthermore exhibits a shoulder at around 1610 cm^{-1} in both experiments, which may indicate the presence of bidentate carbonates during the reaction. In the literature, bands at around 1610 cm^{-1} have been assigned to hydrogen carbonates or bidentate carbonate, but due to the lack of characteristic hydrogen carbonate

bands at 1218 or 1393 cm^{-1}, their presence can be ruled out, thus pointing to the presence of bidentate carbonate.[40,41,44]

Figure 5 shows that for bare ceria the situation is more complex than for gold-loaded samples. When switching on CO_2 (see Figure 5B), the overall trend of all signals in the carbonate region is positive, as in the case of the gold-loaded samples. In particular, in the region between the two intense bands at about 1290 and 1585 cm^{-1} the signals are broader, indicating the presence of more carbonate species during reaction as compared to gold-loaded ceria. In contrast, when switching from CO_2 atmosphere to reaction conditions (see Figure 5A), the signals within 1000–1700 cm^{-1} show a general decrease in intensity, indicating decreased adsorption of CO_2 as carbonates onto the ceria surface. Especially for the sheets, hydrogen carbonates are also present, as evidenced by the characteristic δ(OCOH) vibration at 1217 cm^{-1}, which is most clearly visible in Figure 5B and S6B.[33]

Important mechanistic conclusions can be drawn from the signal at 1943 cm^{-1}, which is only observed for the gold-loaded samples and increases weakly in both experiments, i.e., after switching on CO_2 and H_2 (see Figure 6). Figure 6 provides an enlarged view of the region around 1950 cm^{-1}, together with a spectrum of a Au/sheets sample with 0.62 wt% gold, i.e., about doubled gold loading, showing an intensity increase of the 1943 cm^{-1} feature with increasing gold loading. The 1943 cm^{-1} feature is attributed to Au–H stretching modes of (partially) dissociatively adsorbed hydrogen, as confirmed by our DFT calculations, in which a hydrogen molecule was placed on a gold atom adsorbed on the (111) surface (see Figure S17, structure B), corresponding to the most stable $Au_1/CeO_2(111)$ structure from our previous studies (see Figure S17, structure A).[33] In this case, the calculated H–H distance was 0.93 Å, compared to a distance of 0.75 Å for gas-phase H_2. Based on our experimental observations and DFT results, we propose this state to be stable under reaction conditions only, while in the absence of CO_2, proton transfer to the nearest oxygen atom takes place, leading to immediate formation of a hydroxide and a Au-H species, since this state is energetically preferred by 1.33 eV (see Figure S17, structure C). Such a scenario is fully consistent with the absence of the 1943 cm^{-1} band in H_2 atmosphere, i.e., without CO_2 being present (see Figure S7). In this context, previous studies reported a Au-H species at 2134 cm^{-1}.[27] Remarkably, the 2134 cm^{-1} band is consistent with our DFT calculations and corresponds to a single H atom adsorbed on a gold atom (see Figure S17, structure C), which is detected here for the gold-loaded sheets and polyhedra, lying underneath the signals of gaseous CO (see Figure 6). For pretreatment in H_2 atmosphere the Au-H signal has its maximum at exactly 2134 cm^{-1}, whereas in the case of CO_2 pretreatment, the maximum is detected at about 2110 cm^{-1}. This redshift of the maximum may

be induced by another signal with negative sign, located at about 2164 cm^{-1}, which may originate from adsorbed CO on CeO$_2$(111).[33] This hypothesis is confirmed by spectra of the bare sheets, which show a contribution from CO adsorbates, as will be discussed below. To the best of our knowledge, we have demonstrated the intermediate step of H$_2$ adsorption on gold for the first time. It should be mentioned that we also performed isotope exchange experiments. However, the H$_2$-Au species is not identifiable by D$_2$ isotope exchange as the bands shift into the carbonate/formate region and the H$_2$-Au region is covered by C-D vibrations of formates (not shown). The theoretical H-D shifts are given in Table S2.

Based on the DRIFT spectra in Figure 6, there is no indication for CO adsorbed on gold, since the Au/polyhedra contain larger gold clusters (see above), which would result in IR signals of adsorbed CO below 2100 cm^{-1},[33] and the signals within 2050–2200 cm^{-1} are less pronounced after pretreatment with H$_2$. The latter behavior can be explained by the fact that the signals in this region are assigned to H-Au species (see above), which already exist under the H$_2$ pretreatment and are thus subtracted by the background. It is noteworthy that the band at 1943 cm^{-1} is asymmetric towards higher wavenumbers, possessing a pronounced shoulder at around 2000 cm^{-1}. We propose this behavior to be caused by the presence of larger gold clusters. To confirm this hypothesis, we placed a hydrogen atom on the most stable Au$_4$/CeO$_2$(111) structure from our previous DFT studies (see Figure S17, structure H).[33] The calculations reveal a characteristic band, which is blue shifted by 23 cm^{-1} compared to our single-site structure. Note that this process is endothermic, with an adsorption energy of 0.31 eV (see Table 2). Thus, this state is not preferred, but it is conceivable that the small energy barrier may be overcome at the elevated temperatures of our experiments and a spillover of hydrogen occurs. Further calculations show that H$_2$ interacts only weakly with the Au$_4$ cluster (E$_{ads}$ = –0.1 eV), in contrast to the single-site adsorption energy of –1.08 eV discussed above (see Table S1). Thus, for larger clusters, no hydrogen dissociation on gold is expected; rather, this band is caused by H atoms from H$_2$ adsorption on single Au atoms migrating over the ceria surface. This behavior would also be consistent with experiment, as, based on UV-Vis spectra, the polyhedra contain more metallic gold and thus larger gold clusters (see Figure S3), and these have the most pronounced asymmetry. Regarding the higher 1943 cm^{-1} signal of the polyhedra (despite the presence of larger gold clusters) we point out that, in general, the polyhedra show stronger DRIFTS signals than the sheets (see also Figure 5). Possible reasons for this behavior may be the larger fraction of single Au atoms in the polyhedra, the higher porosity of the sheets, and/or crystal size/shape effects.
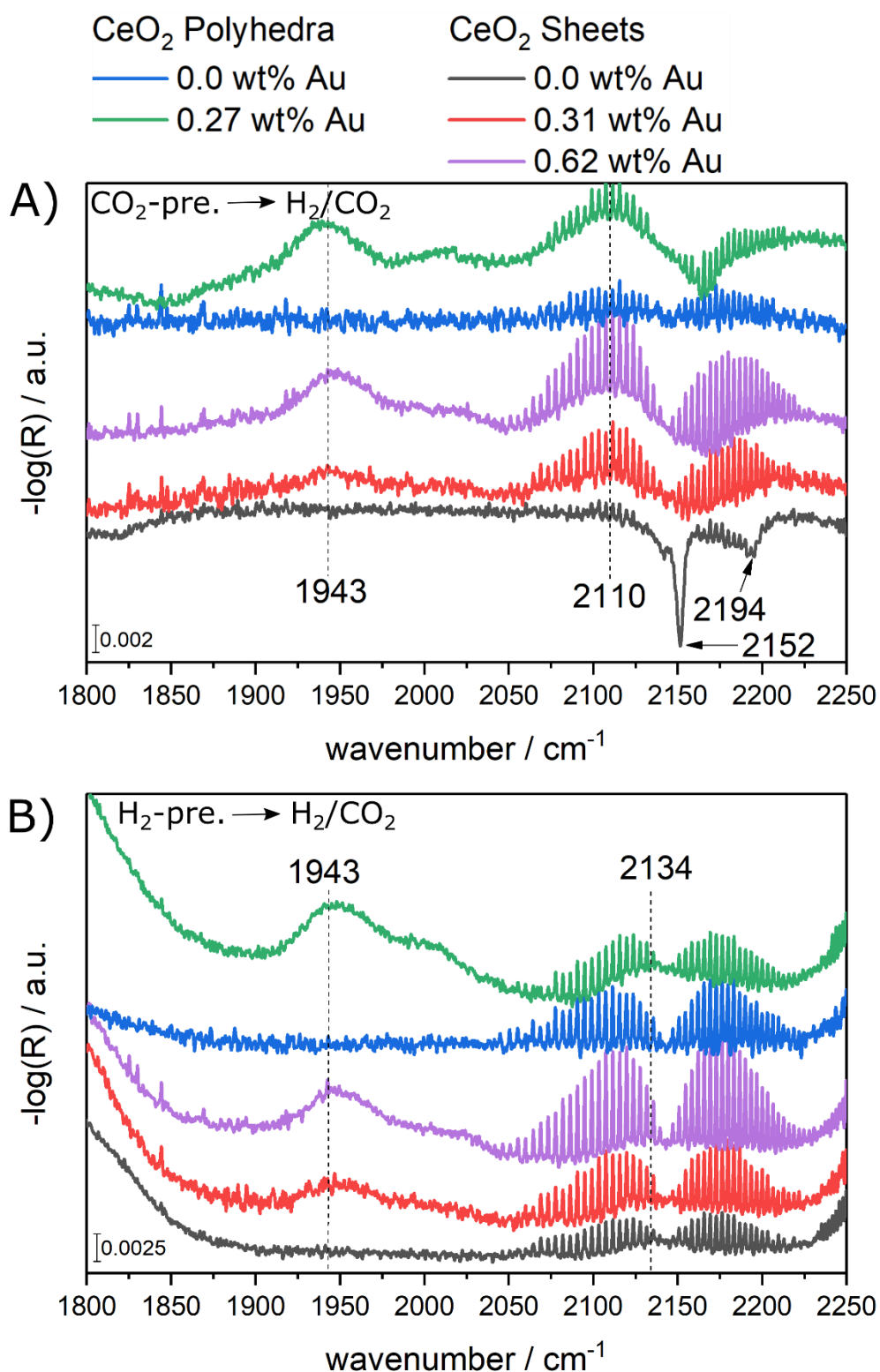
Figure 6: Enlarged view of *in situ* DRIFT spectra from Figure 5 showing the presence of adsorbed hydrogen. Spectra were taken **A)** after the H_2 supply was switched on while CO_2 remained constant, **B)** after the CO_2 supply was switched on while H_2 remained constant. Shown are only the last spectra of a measurement series with a duration of 6 min. For comparison, spectra of Au/CeO_2 sheets with 0.62 wt% gold are shown.

Closer inspection of the transient DRIFT spectra of the bare supports reveals that the sheets exhibit a decreasing feature at 2152 cm^{-1}, which is not detected for the polyhedra (see Figure 6) and only visible after CO_2 pretreatment and addition of H_2. The same behavior is also observed for the switching-off experiments (see Figure S7), i.e., only the bare sheets show an increasing signal at 2152 cm^{-1} after exposure to reaction conditions and after subsequent switching-off of H_2. This signal is assigned to CO adsorbed on CeO_2(111), in agreement with the literature.[45] The fact that it is only detected for the ceria sheets suggests that CO adsorbs more strongly at steps than on the flat CeO_2(111), while exhibiting a similar vibrational frequency. Another interesting observation is that it decreases when H_2 is switched on and increases when H_2 is switched off. Moreover, it remains invisible when CO_2 is switched on after pretreatment in H_2 atmosphere (see Figure 6). Thus the respective surface species seems to be stable only in the absence of H_2. Detailed analysis of the spectra in Figures 5 and 6 reveals that the presence of this CO adsorbate signal correlates with low intensity formate signals in the C–H region at 2838 and 2945 cm^{-1}, in contrast to the ceria polyhedra, which have no adsorbed CO signal and whose format signals are more intense at the same time. This behavior may indicate that formates are not needed as an intermediate in the rWGSR over bare ceria sheets, where stepped sites are present. So, instead of an associative mechanism including formats as intermediates, a redox mechanism involving only surface oxygen atoms may be operative.

Furthermore, at around 2200 cm^{-1} a broad band with increasing intensity is observed for the gold samples in the H_2-on experiment (see Figure 6A), which is not present in the CO_2-on experiment (see Figure 6B). The same inverse behavior for the intensities is also seen for the switching-off experiments (see Figure S7). These observations suggest that these species are not involved in the reaction but are spectator species. In previous studies on Zeolite NaY, bands in this region have been attributed to Au^{3+}-CO species,[46] and such oxidation states of gold are also conceivable on CeO_2(111) if gold occupies a cerium lattice site.[47]

Regarding the bare samples, the sheets show a decreasing band at 2194 cm^{-1}, which is detected in the H_2-on experiment (see Figure 6A) but not in the switching-off experiments (see Figure S7), implying that the related species is not involved in the reaction. Due to the decreasing intensity in the H_2-on and the increasing intensity in the H_2-off experiment, the band does probably not originate from CO adsorbates, which are formed during the reaction, but probably from weakly adsorbed CO_2 on the reduced surface, which has also been detected in the same range on other oxides such as MgO.[48] Its absence in case of the polyhedra suggests that this process may be influenced by steps.

Based on the transient DRIFTS shown in Figure 5, OH species are involved in the reaction. For the gold-loaded samples, increasing O-H stretching signals are observed at about 3528 and 3620 cm^{-1}, and the latter show a stronger increase when the CO_2 feed is switched on. The 3620 cm^{-1} band can be assigned to a triply bonded OH group (type III).[49] Bands at around 3510 cm^{-1} have previously been attributed to a residual oxy-hydroxide phase,[50] but our band is sensitive to the different gas environments. Our DFT calculations have revealed that the dissociation of hydrogen on the gold atom leads to a hydroxide species (see above), which is characterized by a vibrational frequency of 3548 cm^{-1} (Figure S17, structure C). For comparison to the bare support, we have recalculated the most stable hydroxide (H-NNN) from the literature[51] and obtained a vibrational frequency of 3732 cm^{-1}. Based on these findings, we propose the band at 3528 cm^{-1} to originate from hydroxides near gold atoms. Besides, DFT calculations on hydroxides adsorbed on reduced ceria gave significantly higher frequencies than observed here.[50]

In contrast, the intense band at about 3650 cm^{-1} increases in intensity upon addition of H_2 (see Figure 5A), and decreases when CO_2 is switched on (see Figure 5B). This behavior supports previous assignments of this band to O-H stretching of bridged hydroxide in the presence of an oxygen defect on reduced ceria, which has been referred to as OH (II*-B).[50] In addition, a feature at about 3635 cm^{-1} rises under oxidizing conditions (see Figure 5B) and decreases under reducing ones (see Figure 5A), which is consistent with the corresponding hydroxyl species on unreduced surfaces, i.e., OH (II-B).[50]

Water, the only other final product besides CO, might appear in a gaseous or weakly bound surface state. The spectra of bare ceria exhibit only very weak water-related signals due to rotationally resolved gaseous water between 1400 and 2000 cm^{-1}, as well as above 3500 cm^{-1}. For the gold-loaded catalysts, some gaseous water is visible in Figure 5A when H_2 is turned on, whereas weakly bound water can be found as a broad increasing signal, centered around 3300 cm^{-1} (see Figure 5A). Upon addition of CO_2, no weakly bound water is detected and the rotational bands of gaseous water are by far weaker (see Figure 5B). The largely missing water signal may be a result of the pretreatment with hydrogen, which leads to the formation of water, that partially desorbs, thus making it invisible in the difference spectra.[25]

From the transient DRIFT spectra in Figure 5 it is apparent that the type of pretreatment has a pronounced influence on the relative intensities of the individual species. In particular, the formate signals gain considerable intensity upon CO_2 pretreatment (see Figure 5B). On the other hand, the above activity results showed a lower conversion for CO_2 pretreatment than for

H$_2$ pretreatment. Thus, we can already state at this point that the pretreatment has an influence on the reactivity behavior.

4. Discussion of the Reaction Mechanism

Comparing the degree of reduction obtained by the Raman and UV-Vis analysis with the CO$_2$ conversions, it is clear that the reducibility of the support does not play the leading role for the rWGSR activity. In particular, the polyhedra undergo smaller changes during the different gas exposures than the sheets, but exhibit an activity that is higher for the unloaded sample and about the same for the gold-loaded sample. Therefore, a major question concerns the mechanistic role of gold and the ceria support in rWGS over Au/ceria catalysts. Our experimental results, especially the transient DRIFT spectra, show that a different mechanism prevails on the gold-loaded samples than on bare ceria. This is supported by the decreasing intensities of bare ceria in the range below 2000 cm^{-1} (see Figure 5A) and the appearance of additional bands compared to the gold-loaded samples (in this range) when CO$_2$ is turned on (see Figure 5B). A redox mechanism alone cannot explain this behavior. We rather propose that an associative mechanism can occur on the polyhedra even in the absence of gold, which is supported by the formate decomposition (see Figure S6A). Such a behavior is not observed on the sheets. On the other hand, for the sheets, an additional CO-related band is observed at 2152 cm^{-1}, which is not visible for the polyhedra despite the same surface termination, strongly supporting the assumption of a different mechanism on the differently shaped particles. Based on these observations, we propose that on both ceria samples a redox mechanism predominates, but that on the polyhedra also an associative mechanism occurs. In particular, we associate the occurrence of the redox mechanism with the better reducibility of the sheets, originating from the steps. The occurrence of a redox mechanism on both samples is also supported by Figure S14, which shows an increase of CO in the IR gas phase data when switching from H$_2$ to CO$_2$. At the same time, the switch from CO$_2$ to H$_2$ also shows a slight increase in the CO signal for the polyhedra, which is related to the decomposition of remaining carbonaceous adsorbates and thus indicates a reaction pathway via intermediates.

For the gold-loaded samples, an associative mechanism dominates on both samples and is probably facilitated by the easier activation of H$_2$ in the presence of gold. Nevertheless, on the gold-loaded samples a redox mechanism also takes place, as is apparent from switching between oxidizing and reducing conditions, which evidenced the oxidation or reduction of the surface, leading to CO or H$_2$O formation (see Figures 4 and S4). For the rWGSR over Au/TiO$_2$

catalysts a mechanism involving hydroxycarbonyls has been suggested, which we however exclude for Au/ceria, since we do not detect any CO adsorbed on gold, which is essential for the formation of hydroxycarbonyls. Besides, characteristic carboxylate bands are absent,[52] which would indicate the activation of CO_2 on gold. By combining all spectroscopic and theoretical findings of this study, we developed an overall picture of the associative mechanism on the gold-loaded samples, as summarized in Figure 7: Starting with a reduced ceria surface (1), the adsorption of CO_2, facilitated by an oxygen vacancy, leads to carbonate formation (2). Next, carbonate decomposes by release of CO and healing of an oxygen vacancy (3). Reaction of H_2 with surface oxygen results in the formation of water, thereby reducing the surface, while another hydrogen molecule is activated on gold. This activation proceeds in two steps (4). First, a hydrogen molecule dissociatively adsorbs on gold (see Figure S17, structure B), followed by a spillover onto ceria, forming a hydroxide (see Figure S17, structure C), as shown by our combination of experiment and theory. Next, a CO_2 molecule adsorbing onto ceria in the vicinity of gold as carbonate (again facilitated by vacancies), is transformed into formate by hydrogen transport from gold to ceria (5). Finally, formate reacts with a neighboring hydroxide, leading to water and CO formation, thus closing the catalytic cycle. The individual reaction steps are summarized in Figure S16.

We point out that there are two routes by which CO_2 can be activated, i.e., via carbonates or formates/hydroxycarbonyls.[53,54] Theoretical studies[53] indicate that the route via hydroxycarbonyls (COOH) is more competitive than that via formates (HCOO), but based on the absence of specific hydroxycarbonyls bands[55] in our IR experiments, the route via COOH appears to play a minor role. Furthermore, H_2 pretreatment leads to a reduced surface and supports the dissociation of CO_2 to CO via carbonates,[53] which is consistent with our observation of higher activities after H_2 pretreatment and the lower C-H signals in Figure 5B. This step is also proposed to be rate-determining, since the healing of defects by CO_2 via the release of CO (CeO_2(111) without gold) is endothermic by 0.98 eV. Based on our findings, the formate and carbonate formation steps (5, 2) cannot be explicitly separated from each other, thus these steps may run independently of each other. For example, by omitting steps 2 and 3, the reaction may proceed directly to step 4. This is also consistent with the higher C–H intensities in the measurements with CO_2 pretreatment (see Figure 5A), which are starting from a more oxidized surface compared to the H_2 pretreatment. Studies during methane dry reforming over [18]O labeled Ni/CeO_2 have shown, that lattice oxygen is involved in the formation of CO.[56] However, in the reaction discussed here, no coking of the catalyst can be detected, so the involvement of lattice oxygen in CO formation similar to methane dry

reforming is improbable. Nevertheless, such studies could support the involvement of lattice oxygen in the formation of H_2O. In summary, the CO_2 reduction pathway depends on the concentration of defects and/or hydroxides, which in turn depend on the pretreatment (see also Figure S13). Thus, on a defect-rich surface (H_2 pretreatment), the path via carbonates is preferred, while on the other hand, on a surface with fewer defects, the path via formates will dominate.
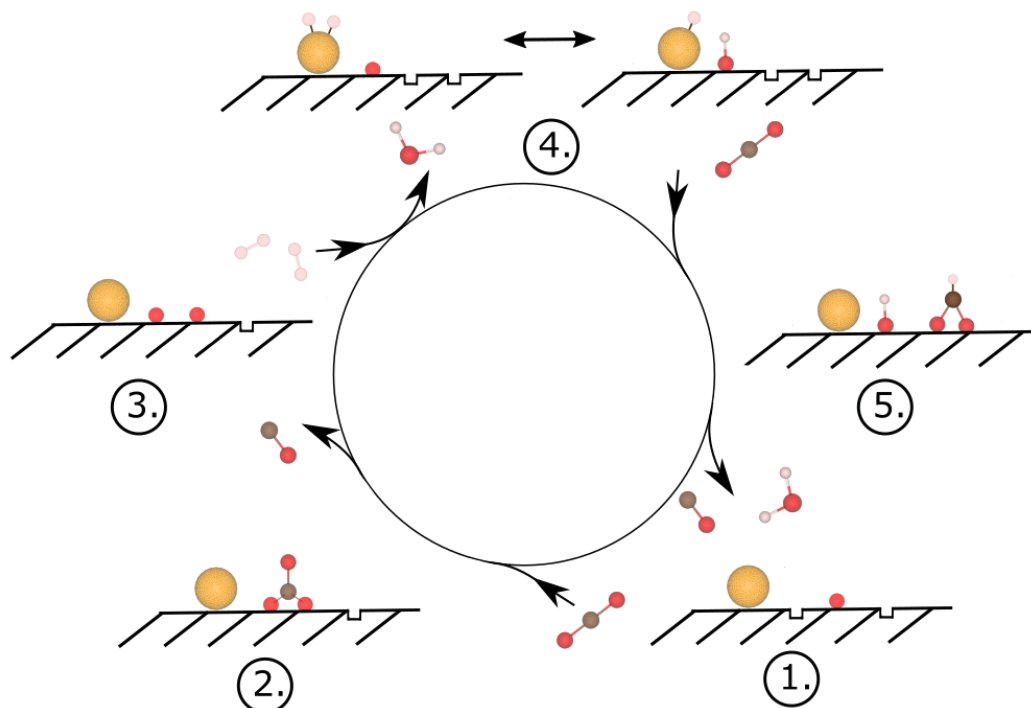

Figure 7: Proposed mechanism for the reverse water–gas shift reaction (rWGSR) over $Au/CeO_2(111)$ catalysts. For clarity, only the reaction pathway mediated by a gold single site is shown. Atoms correspond to oxygen (red), carbon (brown), hydrogen (white) and gold (gold).

5. Conclusions

Based on the *operando* Raman and UV-Vis spectroscopic observations, the ability to form defects plays a minor role in the conversion of CO_2 within the rWGSR. Indeed, when the reducibility of the gold-loaded samples is compared, sheets undergo significantly larger changes under reducing (H_2) or reaction conditions (see Figure 3), while their activity is very similar to that of the polyhedra (see Table 1). These observations are evidence of the fact that defect formation is not essential for the reaction pathway and that the route via intermediates (formates, carbonates, hydroxides) is more important. However, detailed analysis reveals that the pretreatment (H_2, CO_2) has an influence on the reaction pathway and on the catalytic

activity. To this end, CO_2 reduction over a reduced ceria surface favors carbonate intermediates, while over a low-defect surface a reduction via formates is preferred; besides, starting from a highly reduced surface (H_2 pretreatment) leads to higher activities.

In contrast to bare ceria, a pure redox mechanism loses importance on Au/ceria catalysts at lower temperatures ($\leq$250 °C). This is attributed to the activation of hydrogen on gold atoms, whereas hydrogen interacts in its molecular form only very weakly with the bare CeO_2(111) surface.[51] In this context, using transient DRIFTS in combination with DFT calculations, we were able to elucidate for the first time the individual steps of H_2 activation over Au/CeO_2(111), which is shown to proceed in two steps (see Figure 8). Based on our findings, we propose gold atoms to be essential for an associative mechanism.

Our study clearly reveals that multiple techniques, sampling both subsurface and surface properties, are required to elucidate the mechanism of the rWGSR over Au/CeO_2 catalysts. In particular, the use of *operando* and transient approaches in combination with theory is shown to enable a detailed analysis, including spectroscopic features not reported in the literature.

Supporting Information

Detailed information on experimental and theoretical methods as well as additional experimental and theoretical data.

References

[1]   J. Jiang, B. Ye, J. Liu, Research on the peak of CO_2 emissions in the developing world: Current progress and future prospect, Appl. Energy. 235 (2019) 186–203. https://doi.org/10.1016/j.apenergy.2018.10.089.

[2]   X. Chen, Y. Chen, C. Song, P. Ji, N. Wang, W. Wang, L. Cui, Recent Advances in Supported Metal Catalysts and Oxide Catalysts for the Reverse Water-Gas Shift Reaction, Front. Chem. 8 (2020) 1–21. https://doi.org/10.3389/fchem.2020.00709.

[3]   M. Boaro, S. Colussi, A. Trovarelli, Ceria-Based Materials in Hydrogenation and Reforming Reactions for CO_2 Valorization, Front. Chem. 7:28 (2019). https://doi.org/10.3389/fchem.2019.00028.

[4]   K. Chang, H. Zhang, M. Cheng, Q. Lu, Application of Ceria in CO_2 Conversion Catalysis, ACS Catal. 10 (2020) 613–631. https://doi.org/10.1021/acscatal.9b03935.

[5]   G. Jacobs, B.H. Davis, Reverse water-gas shift reaction: steady state isotope switching study of the reverse water-gas shift reaction using in situ DRIFTS and a Pt/ceria catalyst, Appl. Catal. A Gen. 284 (2005) 31–38. https://doi.org/10.1016/j.apcata.2005.01.013.

[6]   F.C. Meunier, D. Tibiletti, A. Goguet, D. Reid, R. Burch, On the reactivity of carbonate species on a Pt/CeO_2 catalyst under various reaction atmospheres: Application of the isotopic exchange technique, Appl. Catal. A Gen. 289 (2005) 104–112. https://doi.org/10.1016/j.apcata.2005.04.018.

[7]   C.M. Kalamaras, S. Americanou, A.M. Efstathiou, "Redox" vs "associative formate with –OH group regeneration" WGS reaction mechanism on Pt/CeO_2: Effect of platinum particle size, J. Catal. 279 (2011) 287–300. https://doi.org/10.1016/j.jcat.2011.01.024.

[8]   L. Lin, S. Yao, Z. Liu, F. Zhang, N. Li, D. Vovchok, A. Martínez-Arias, R. Castañeda, J. Lin, S.D. Senanayake, D. Su, D. Ma, J.A. Rodriguez, In Situ Characterization of Cu/CeO_2 Nanocatalysts for CO_2 Hydrogenation: Morphological Effects of Nanostructured Ceria on the Catalytic Activity, J. Phys. Chem. C. 122 (2018) 12934–12943. https://doi.org/10.1021/acs.jpcc.8b03596.

[9]   Y. Liu, Z. Li, H. Xu, Y. Han, Reverse water-gas shift reaction over ceria nanocube synthesized by hydrothermal method, Catal. Commun. 76 (2016) 1–6. https://doi.org/10.1016/j.catcom.2015.12.011.

[10]   L.F. Bobadilla, J.L. Santos, S. Ivanova, J.A. Odriozola, A. Urakawa, Unravelling the Role of Oxygen Vacancies in the Mechanism of the Reverse Water–Gas Shift Reaction by Operando DRIFTS and Ultraviolet–Visible Spectroscopy, ACS Catal. 8 (2018) 7455–7467. https://doi.org/10.1021/acscatal.8b02121.

[11]   J.A. Rodríguez, J. Evans, J. Graciani, J.-B. Park, P. Liu, J. Hrbek, J.F. Sanz, High Water−Gas Shift Activity in TiO_2(110) Supported Cu and Au Nanoparticles: Role of

the Oxide and Metal Particle Size, J. Phys. Chem. C. 113 (2009) 7364–7370. https://doi.org/10.1021/jp900483u.

[12] L.C. Wang, M. Tahvildar Khazaneh, D. Widmann, R.J. Behm, TAP reactor studies of the oxidizing capability of CO_2 on a Au/CeO_2 catalyst – A first step toward identifying a redox mechanism in the Reverse Water–Gas Shift reaction, J. Catal. 302 (2013) 20–30. https://doi.org/10.1016/j.jcat.2013.02.021.

[13] L.C. Wang, D. Widmann, R.J. Behm, Reactive removal of surface oxygen by H_2, CO and CO/H_2 on a Au/CeO_2 catalyst and its relevance to the preferential CO oxidation (PROX) and reverse water gas shift (RWGS) reaction, Catal. Sci. Technol. 5 (2015) 925–941. https://doi.org/10.1039/C4CY01030B.

[14] C. Schilling, C. Hess, Elucidating the Role of Support Oxygen in the Water–Gas Shift Reaction over Ceria-Supported Gold Catalysts Using Operando Spectroscopy, ACS Catal. 9 (2019) 1159–1171. https://doi.org/10.1021/acscatal.8b04536.

[15] M. Ziemba, M.V. Ganduglia-Pirovano, C. Hess, Insight into the mechanism of the water–gas shift reaction over Au/CeO_2 catalysts using combined operando spectroscopies, Faraday Discuss. 229 (2021) 232–250. https://doi.org/10.1039/C9FD00133F.

[16] X. Fu, L. Guo, W. Wang, C. Ma, C. Jia, K. Wu, R. Si, L.-D. Sun, C.-H. Yan, Direct Identification of Active Surface Species for the Water–Gas Shift Reaction on a Gold–Ceria Catalyst, J. Am. Chem. Soc. (2019) jacs.8b09306. https://doi.org/10.1021/jacs.8b09306.

[17] A.M. Efstathiou, Catalysis, Royal Society of Chemistry, Cambridge, 2016. https://doi.org/10.1039/9781782626855.

[18] T. Staudt, Y. Lykhach, N. Tsud, T. Skála, K.C. Prince, V. Matolín, J. Libuda, Ceria reoxidation by CO_2: A model study, J. Catal. 275 (2010) 181–185. https://doi.org/10.1016/j.jcat.2010.07.032.

[19] S. Ackermann, L. Sauvin, R. Castiglioni, J.L.M. Rupp, J.R. Scheffe, A. Steinfeld, Kinetics of CO_2 Reduction over Nonstoichiometric Ceria, J. Phys. Chem. C. 119 (2015) 16452–16461. https://doi.org/10.1021/acs.jpcc.5b03464.

[20] J.A. Rodriguez, D.C. Grinter, Z. Liu, R.M. Palomino, S.D. Senanayake, Ceria-based model catalysts: Fundamental studies on the importance of the metal-ceria interface in CO oxidation, the water-gas shift, CO_2 hydrogenation, and methane and alcohol reforming, Chem. Soc. Rev. 46 (2017) 1824–1841. https://doi.org/10.1039/c6cs00863a.

[21] J.H. Carter, G.J. Hutchings, Recent Advances in the Gold-Catalysed Low-Temperature

Water–Gas Shift Reaction, Catalysts. 8 (2018) 627.
https://doi.org/10.3390/catal8120627.

[22] A.M. Abdel-Mageed, G. Kučerova, J. Bansmann, R.J. Behm, Active Au species during the low-temperature water gas shift reaction on Au/CeO$_2$: A time-resolved operando XAS and DRIFTS study, ACS Catal. 7 (2017) 6471–6484.
https://doi.org/10.1021/acscatal.7b01563.

[23] J.H. Carter, X. Liu, Q. He, S. Althahban, E. Nowicka, S.J. Freakley, L. Niu, D.J. Morgan, Y. Li, J.W.H. Niemantsverdriet, S. Golunski, C.J. Kiely, G.J. Hutchings, Activation and Deactivation of Gold/Ceria-Zirconia in the Low-Temperature Water-Gas Shift Reaction, Angew. Chem. Int. Ed. 56 (2017) 16037–16041.
https://doi.org/10.1002/anie.201709708.

[24] A.M. Efstathiou, K.C. Petallidou, Reply to the Letter to the Editor concerning the comments of Dr. F. Meunier to the article Appl. Catal. B: Environ. 136–137 (2013) 225–238, Kalamaras et al., titled "The effect of La^{3+}-doping of CeO$_2$ support on the water–gas shift re, Appl. Catal. B Environ. 152–153 (2014) 439–443.
https://doi.org/10.1016/j.apcatb.2014.01.064.

[25] D. Schweke, L. Shelly, R. Ben David, A. Danon, N. Kostirya, S. Hayun, Comprehensive Study of the Ceria–H$_2$ System: Effect of the Reaction Conditions on the Reduction Extent and Intermediates, J. Phys. Chem. C. 124 (2020) 6180–6187.
https://doi.org/10.1021/acs.jpcc.9b11975.

[26] Z. Wu, Y. Cheng, F. Tao, L. Daemen, G.S. Foo, L. Nguyen, X. Zhang, A. Beste, A.J. Ramirez-Cuesta, Direct Neutron Spectroscopy Observation of Cerium Hydride Species on a Cerium Oxide Catalyst, J. Am. Chem. Soc. 139 (2017) 9721–9727.
https://doi.org/10.1021/jacs.7b05492.

[27] R. Juárez, S.F. Parker, P. Concepción, A. Corma, H. García, Heterolytic and heterotopic dissociation of hydrogen on ceria-supported gold nanoparticles. Combined inelastic neutron scattering and FT-IR spectroscopic study on the nature and reactivity of surface hydrogen species, Chem. Sci. 1 (2010) 731.
https://doi.org/10.1039/c0sc00336k.

[28] D. Ren, L. He, L. Yu, R.-S. Ding, Y.-M. Liu, Y. Cao, H.-Y. He, K.-N. Fan, An Unusual Chemoselective Hydrogenation of Quinoline Compounds Using Supported Gold Catalysts, J. Am. Chem. Soc. 134 (2012) 17592–17598.
https://doi.org/10.1021/ja3066978.

[29] H.Y. Kim, G. Henkelman, CO Oxidation at the Interface of Au Nanoclusters and the

Stepped-CeO$_2$(111) Surface by the Mars–van Krevelen Mechanism, J. Phys. Chem. Lett. 4 (2013) 216–221. https://doi.org/10.1021/jz301778b.

[30] C. Schilling, C. Hess, CO Oxidation on Ceria Supported Gold Catalysts Studied by Combined Operando Raman/UV–Vis and IR Spectroscopy, Top. Catal. 60 (2017) 131–140. https://doi.org/10.1007/s11244-016-0732-6.

[31] C. Schilling, M.V. Ganduglia-Pirovano, C. Hess, Experimental and Theoretical Study on the Nature of Adsorbed Oxygen Species on Shaped Ceria Nanoparticles, J. Phys. Chem. Lett. 9 (2018) 6593–6598. https://doi.org/10.1021/acs.jpclett.8b02728.

[32] M. Ziemba, C. Hess, Influence of gold on the reactivity behaviour of ceria nanorods in CO oxidation: combining operando spectroscopies and DFT calculations, Catal. Sci. Technol. 10 (2020) 3720–3730. https://doi.org/10.1039/D0CY00392A.

[33] C. Schilling, M. Ziemba, C. Hess, M.V. Ganduglia-Pirovano, Identification of single-atom active sites in CO oxidation over oxide-supported Au catalysts, J. Catal. 383 (2020) 264–272. https://doi.org/10.1016/j.jcat.2020.01.022.

[34] A. Goguet, F.C. Meunier, D. Tibiletti, J.P. Breen, R. Burch, Spectrokinetic Investigation of Reverse Water-Gas-Shift Reaction Intermediates over a Pt/CeO$_2$ Catalyst, J. Phys. Chem. B. 108 (2004) 20240–20246. https://doi.org/10.1021/jp047242w.

[35] C.W.M. Castleton, J. Kullgren, K. Hermansson, Tuning LDA+U for electron localization and structure at oxygen vacancies in ceria, J. Chem. Phys. 127 (2007) 244704. https://doi.org/10.1063/1.2800015.

[36] J.A. Hernández, S.A. Gómez, T.A. Zepeda, J.C. Fierro-González, G.A. Fuentes, Insight into the Deactivation of Au/CeO$_2$ Catalysts Studied by In Situ Spectroscopy during the CO-PROX Reaction, ACS Catal. 5 (2015) 4003–4012. https://doi.org/10.1021/acscatal.5b00739.

[37] C. Schilling, A. Hofmann, C. Hess, M.V. Ganduglia-Pirovano, Raman Spectra of Polycrystalline CeO$_2$: A Density Functional Theory Study, J. Phys. Chem. C. 121 (2017) 20834–20849. https://doi.org/10.1021/acs.jpcc.7b06643.

[38] A.M. Abdel-Mageed, G. Kučerová, J. Bansmann, R.J. Behm, Active Au Species During the Low-Temperature Water Gas Shift Reaction on Au/CeO$_2$: A Time-Resolved Operando XAS and DRIFTS Study, ACS Catal. 7 (2017) 6471–6484. https://doi.org/10.1021/acscatal.7b01563.

[39] V. Marchionni, D. Ferri, O. Kröcher, A. Wokaun, Increasing the Sensitivity to Short-Lived Species in a Modulated Excitation Experiment, Anal. Chem. 89 (2017) 5801–

5809. https://doi.org/10.1021/acs.analchem.6b04939.

[40]   G.N. Vayssilov, M. Mihaylov, P.S. Petkov, K.I. Hadjiivanov, K.M. Neyman, Reassignment of the Vibrational Spectra of Carbonates, Formates, and Related Surface Species on Ceria: A Combined Density Functional and Infrared Spectroscopy Investigation, J. Phys. Chem. C. 115 (2011) 23435–23454. https://doi.org/10.1021/jp208050a.

[41]   F. Romero-Sarria, L.M. Martínez T, M.A. Centeno, J.A. Odriozola, Surface Dynamics of Au/CeO_2 Catalysts during CO Oxidation, J. Phys. Chem. C. 111 (2007) 14469–14475. https://doi.org/10.1021/jp073541k.

[42]   D. Vovchok, C. Zhang, S. Hwang, L. Jiao, F. Zhang, Z. Liu, S.D. Senanayake, J.A. Rodriguez, Deciphering Dynamic Structural and Mechanistic Complexity in Cu/CeO_2/ZSM-5 Catalysts for the Reverse Water-Gas Shift Reaction, ACS Catal. 10 (2020) 10216–10228. https://doi.org/10.1021/acscatal.0c01584.

[43]   W.O. Gordon, Y. Xu, D.R. Mullins, S.H. Overbury, Temperature evolution of structure and bonding of formic acid and formate on fully oxidized and highly reduced CeO_2(111), Phys. Chem. Chem. Phys. 11 (2009) 11171. https://doi.org/10.1039/b913310k.

[44]   Y. Denkwitz, A. Karpenko, V. Plzak, R. Leppelt, B. Schumacher, R.J. Behm, Influence of CO_2 and H_2 on the low-temperature water–gas shift reaction on Au/CeO_2 catalysts in idealized and realistic reformate, J. Catal. 246 (2007) 74–90. https://doi.org/10.1016/j.jcat.2006.11.012.

[45]   C. Wöll, Structure and Chemical Properties of Oxide Nanoparticles Determined by Surface-Ligand IR Spectroscopy, ACS Catal. (2019) acscatal.9b04016. https://doi.org/10.1021/acscatal.9b04016.

[46]   M.Y. Mihaylov, J.C. Fierro-Gonzalez, H. Knözinger, B.C. Gates, K.I. Hadjiivanov, Formation of Nonclassical Carbonyls of Au^{3+} in Zeolite NaY: Characterization by Infrared Spectroscopy, J. Phys. Chem. B. 110 (2006) 7695–7701. https://doi.org/10.1021/jp057426q.

[47]   M.F. Camellone, S. Fabris, Reaction Mechanisms for the CO Oxidation on Au/CeO_2 Catalysts: Activity of Substitutional Au^{3+}/Au^+ Cations and Deactivation of Supported Au^+ Adatoms, J. Am. Chem. Soc. 131 (2009) 10473–10483. https://doi.org/10.1021/ja902109k.

[48]   I.M. Hill, S. Hanspal, Z.D. Young, R.J. Davis, DRIFTS of Probe Molecules Adsorbed on Magnesia, Zirconia, and Hydroxyapatite Catalysts, J. Phys. Chem. C. 119 (2015)

9186–9197. https://doi.org/10.1021/jp509889j.

[49] A. Laachir, V. Perrichon, A. Badri, J. Lamotte, E. Catherine, J.C. Lavalley, J. El Fallah, L. Hilaire, F. Le Normand, E. Quéméré, G.N. Sauvion, O. Touret, Reduction of CeO_2 by hydrogen. Magnetic susceptibility and Fourier-transform infrared, ultraviolet and X-ray photoelectron spectroscopy measurements, J. Chem. Soc. Faraday Trans. 87 (1991) 1601–1609. https://doi.org/10.1039/FT9918701601.

[50] A. Badri, C. Binet, J. Lavalley, An FTIR study of surface ceria hydroxy groups during a redox process with H_2, J. Chem. Soc. Faraday Trans. 92 (1996) 4669. https://doi.org/10.1039/ft9969204669.

[51] D. Fernández-Torre, J. Carrasco, M.V. Ganduglia-Pirovano, R. Pérez, Hydrogen activation, diffusion, and clustering on $CeO_2(111)$: A DFT+ U study, J. Chem. Phys. 141 (2014) 014703. https://doi.org/10.1063/1.4885546.

[52] E.T. Saw, U. Oemar, M.L. Ang, H. Kus, S. Kawi, High-temperature water gas shift reaction on Ni–Cu/CeO_2 catalysts: effect of ceria nanocrystal size on carboxylate formation, Catal. Sci. Technol. 6 (2016) 5336–5349. https://doi.org/10.1039/C5CY01932J.

[53] X. Lu, W. Wang, S. Wei, C. Guo, Y. Shao, M. Zhang, Z. Deng, H. Zhu, W. Guo, Initial reduction of CO_2 on perfect and O-defective $CeO_2(111)$ surfaces: Towards CO or COOH?, RSC Adv. 5 (2015) 97528–97535. https://doi.org/10.1039/c5ra17825h.

[54] Y. Yang, S. Wang, Y. Jiang, X. Wu, C. Xia, R. Peng, Y. Lu, CO_2 Activation and Reduction on Pt-CeO_2-Based Catalysts, J. Phys. Chem. C. 123 (2019) 17092–17101. https://doi.org/10.1021/acs.jpcc.9b02878.

[55] O. Pozdnyakova, D. Teschner, A. Wootsch, J. Krohnert, B. Steinhauer, H. Sauer, L. Toth, F. Jentoft, A. Knopgericke, A. Knopgericke, Z. Paal, Preferential CO oxidation in hydrogen (PROX) on ceria-supported catalysts, part I: Oxidation state and surface species on Pt/CeO_2 under reaction conditions, J. Catal. 237 (2006) 1–16. https://doi.org/10.1016/j.jcat.2005.10.014.

[56] C.M. Damaskinos, J. Zavašnik, P. Djinović, A.M. Efstathiou, Dry reforming of methane over Ni/$Ce_{0.8}Ti_{0.2}O_{2-\delta}$: The effect of Ni particle size on the carbon pathways studied by transient and isotopic techniques, Appl. Catal. B Environ. 296 (2021) 120321. https://doi.org/10.1016/j.apcatb.2021.120321.